Mineralogical effects on the detectability of the postperovskite boundary

Brent Grocholski[a,1], Krystle Catalli[a], Sang-Heon Shim[a], and Vitali Prakapenka[b]

[a]Department of Earth, Atmospheric, and Planetary Science, Massachusetts Institute of Technology, 77 Massachusetts Avenue, Cambridge, MA 02139; and [b]Center for Advanced Radiation Sources, University of Chicago, 5640 South Ellis Avenue, Chicago, IL 60637

Edited by Russell J. Hemley, Carnegie Institution of Washington, Washington, DC, and approved December 23, 2011 (received for review June 14, 2011)

The discovery of a phase transition in Mg-silicate perovskite (Pv) to postperovskite (pPv) at lowermost mantle pressure-temperature ($P-T$) conditions may provide an explanation for the discontinuous increase in shear wave velocity found in some regions at a depth range of 200 to 400 km above the core-mantle boundary, hereafter the D″ discontinuity. However, recent studies on binary and ternary systems showed that reasonable contents of Fe^{2+} and Al for pyrolite increase the thickness (width of the mixed phase region) of the Pv – pPv boundary (400–600 km) to much larger than the D″ discontinuity (≤70 km). These results challenge the assignment of the D″ discontinuity to the Pv – pPv boundary in pyrolite (homogenized mantle composition). Furthermore, the mineralogy and composition of rocks that can host a detectable Pv → pPv boundary are still unknown. Here we report in situ measurements of the depths and thicknesses of the Pv → pPv transition in multiphase systems (San Carlos olivine, pyrolitic, and midocean ridge basaltic compositions) at the $P-T$ conditions of the lowermost mantle, searching for candidate rocks with a sharp Pv – pPv discontinuity. Whereas the pyrolitic mantle may not have a seismologically detectable Pv → pPv transition due to the effect of Al, harzburgitic compositions have detectable transitions due to low Al content. In contrast, Al-rich basaltic compositions may have a detectable Pv – pPv boundary due to their distinct mineralogy. Therefore, the observation of the D″ discontinuity may be related to the Pv → pPv transition in the differentiated oceanic lithosphere materials transported to the lowermost mantle by subducting slabs.

The lower mantle is a multicomponent (MgO, SiO_2, FeO, Al_2O_3, CaO, Na_2O, etc.), multiphase (magnesium silicate perovskite (Pv), ferropericlase (Fp), calcium silicate perovskite (Ca-Pv), silica, calcium-ferrite-type aluminous (CF) phase, etc.) system and understanding the effects of chemistry and mineralogy on the depths and thicknesses of mantle phase boundaries is of fundamental interest. Although the discovery of the Pv → pPv transition at lowermost mantle $P-T$ conditions (1–3) has been invoked as an explanation for the D″ discontinuity, the combined effect of mineralogy and chemistry remain unresolved. Some recent studies (4–14) demonstrated large effects of chemical composition on the depth and thickness of the Pv → pPv boundary. The depth range over which the Pv → pPv transition occurs in mantle-related systems is much wider (4, 5) than the seismically constrained thickness (15, 16). It also occurs close to the core-mantle boundary (CMB) (135 GPa) even at 2,500 K with a positive Clapeyron slope, making it possible that the transition may not occur at all in the hotter lowermost mantle. Although the effect of Fp on the Pv → pPv transition has been modeled (4), other mineralogical effects are not fully understood due in part to our poor understanding of Al partitioning in these systems. Direct measurements on different mantle-related compositions are critical in determining the source of the seismically detectable Pv – pPv boundary.

Here we report in situ measurements on the depth and thickness of the Pv – pPv boundary in San Carlos olivine, pyrolitic, and midocean ridge basaltic (MORB) compositions conducted in the double-sided laser-heated diamond-anvil cell at pressures up to 170 GPa and temperatures up to 3,000 K. We loaded compressible Ar or Ne as a pressure transmitting medium, which also acts as an insulation medium to reduce thermal gradients. To further decrease the radial thermal gradients, we made the size of the sample platelet comparable to the size of the laser beam focus. Samples were heated for long durations at given pressures (1–1.5 h), and the boundary was measured during compression and decompression (reversal) to reduce kinetic problems. These improvements over previous studies allow us to obtain a reliable dataset to extract chemical and mineralogical effects on the properties of the Pv – pPv boundary. The methods we used are identical to those in Catalli et al. (4), and further discussed below and in *Supporting Information*.

Results

Laser heating of pyrolitic material at lowermost mantle pressures produces approximately 70 mol% Mg-silicate (Pv and/or pPv) and approximately 30 mol% Fp (Fig. 1 *A*–*C*). Among the major oxide components, we do not include CaO in our pyrolitic starting material to avoid the diffraction peaks of Ca-Pv. Ca-Pv is not capable of influencing the depth or thickness of the Pv → pPv transition because it comprises only 5 mol% and remains chemically pure in pyrolite according to Murakami et al. (17) (*Supporting Information*). Two samples of pyrolitic starting material were heated to 1,600–2,500 K at 124 and 130 GPa with the diffraction lines of Pv and Fp appearing within the first 10 min of heating (Fig. 1*A*). Pv remains stable up to 139 GPa at high temperature. Three pyrolite samples were heated at 139, 145, and 165 GPa, producing Pv + pPv that remains stable throughout heating (Fig. 1*B*). We compressed or decompressed the samples between 130 and 158 GPa and found that Pv + pPv continues to be stable assemblage. A sixth sample heated to 2,400 K at 170 GPa crystallized pure pPv with Fp within the first 10 min of heating (Fig. 1*C*).

Compared with the pyrolitic sample, San Carlos olivine produces a greater amount of Fp (50 mol% Mg-silicate and 50 mol % Fp). A pressure-amorphized olivine sample heated to 2,000–3,000 K at 128–133 GPa crystallized pure Pv with Fp that remains stable throughout heating (Fig. 1*D*). Another sample was heated to 2,700–3,000 K at 135 GPa, producing a mixture of Pv + pPv (Fig. 1*E*). A third sample was heated at 2,500 K and 136 GPa, where pure pPv was synthesized and remained stable throughout heating. This sample was decompressed and heated at different pressures. The pPv → Pv boundary was inferred by the appearance of Pv lines along with the broadening and decrease in the intensity of pPv lines after decompression and heating at 117 GPa. A fourth sample was heated at approximately 3,000 K and 140 GPa, producing pure pPv. The sample was then decompressed to 123 GPa,

Author contributions: B.G., K.C., and S.-H.S. designed research; B.G., K.C., and S.-H.S. performed research; B.G., K.C., S.-H.S., and V.B.P. contributed new reagents/analytic tools; B.G., K.C., and S.-H.S. analyzed data; and B.G., K.C., and S.-H.S. wrote the paper.

The authors declare no conflict of interest.

This article is a PNAS Direct Submission.

[1]To whom correspondence should be addressed. E-mail: b.grocholski@gmail.com.

This article contains supporting information online at www.pnas.org/lookup/suppl/doi:10.1073/pnas.1109204109/-/DCSupplemental.

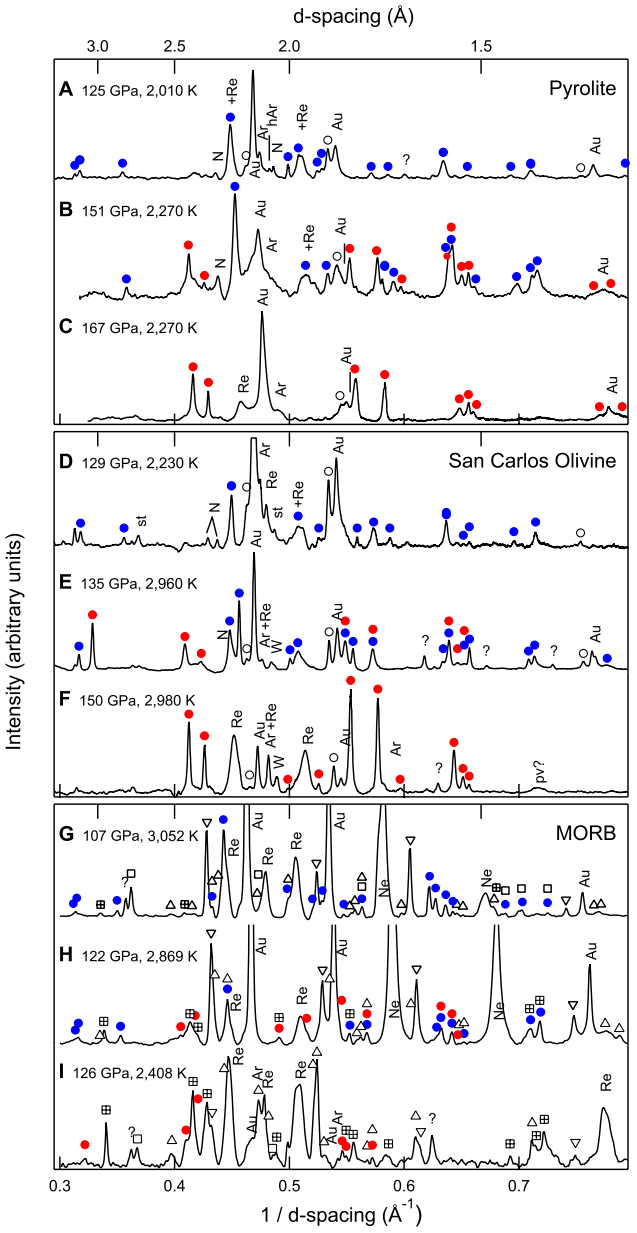

Fig. 1. X-ray diffraction patterns of (*A–C*) Ca-free pyrolitic, (*D–F*) San Carlos olivine, and (*G–I*) MORB compositions measured at high pressure and temperature. The major peaks are indicated for Pv (blue circles), pPv (red circles), Fp (open circles), $CaCl_2$-type silica (open square), α-PbO_2-type silica (square with cross), CF phase (open up triangle), Ca-Pv (open down triangle), the gold internal pressure calibrant (Au), rhenium gasket (Re), argon or neon pressure medium (Ar or Ne), and nitrogen (N). A few unidentified lines are noted by "?" (*Supporting Information*). Backgrounds were subtracted. The diffraction intensities are plotted as a function of inverse interplanar distance.

where an unheated sample spot was located and heated at 2,700 K, forming pure Pv together with Fp.

Based on the relative peak intensities in our diffraction patterns, electron probe microanalysis (EPMA) of the starting glass, and a previous study (18), the MORB sample should contain approximately 35 mol% Mg-silicate, approximately 35 mol% silica, approximately 20 mol% Ca-Pv, and approximately 10 mol% CF-type phase at lowermost mantle conditions (Fig. 1 *G–I*). Ca-Pv produces the dominant lines in the diffraction patterns of MORB at lower-mantle pressures due to its higher symmetry. Pv forms together with other phases in starting material heated to 105 GPa and 3,000 K. Pressure was then increased to 114 GPa and heated to 2,800 K, where diffractions peaks for pPv grew and coexisted with Pv, indicating the Pv → Pv + pPv boundary. A second sample was taken to 100 GPa and 2,500 K, with Pv again found to be stable without pPv. A third MORB sample produced Pv + pPv when heated at 115 GPa and 2,600 K. The sample was then decompressed to 95 GPa and 2,600 K where Pv diffraction peaks grew and the pPv phase disappeared, indicating the stability of Pv. Separate samples heated at 118 GPa and 122 GPa and 3,000 K produced Pv + pPv. Pure pPv was formed in a fresh sample at 126 GPa and 2,500 K, and remained stable throughout heating (for a detailed description on these observations refer to *Supporting Information*).

Discussion

The pressure-temperature conditions of our data points obtained through two different in situ methods are shown in Fig. 2: synthesis of stable phase assemblages (method A) from previously unheated amorphous starting materials within 20 min of heating (large circles), and (method B) from previously heated Pv, pPv, or Pv + pPv for 60–90 min of heating (triangles). Method A has been used in most pPv boundary studies, whereas no previous studies attempted method B for the multicomponent systems. Kinetic problems should be less severe from method A because the data points are obtained from a highly metastable state. Also, Soret diffusion may be less severe in the short laser heating of method A. However, laser heating of highly metastable materials in this method could result in the synthesis of a metastable phase assemblage at a local energy minimum, particularly under severe deviatoric stresses or temperature gradients. Many previous studies used a NaCl medium, which becomes much less compressible after the B1–B2 phase transition, or even no medium for pressure transmission and thermal insulation.

Although a metastable assemblage is less likely synthesized in method B where we used a crystalline phase assemblage stable in an adjacent $P-T$ field as a starting material, it may be more severely affected by kinetics under poor thermal insulation with insufficient heating duration. However, we measured the boundary along both the forward and reverse directions (reversal) and achieved more stable heating with thermal insulation and longer heating duration, which is important to reduce the kinetic issues.

Although we made efforts to reduce the experimental issues in the laser-heated diamond-anvil cell (e.g., deviatoric stresses, thermal gradients, Soret diffusion, and kinetics), problems may still exist and could introduce some error in our data points. Therefore, it is important to examine the severity of those issues. Comparison of the boundary determination results from methods A and B, which are complementary to each other, should provide an important test. As shown in Fig. 2, these two methods yield consistent depths and thicknesses of the phase boundaries within approximately 10 GPa.

Our reversal measurements (*Supporting Information*) also provide an estimate for kinetic effects. Difference in the boundaries determined during the forward and reverse directions is less than 8 GPa (≤150 km) in these multiphase systems. Although this is larger than in the binary and ternary systems studied in Catalli et al. (4), suggesting larger kinetic effects are likely due to the sluggish redistribution of cations amongst the different phases in the multiphase systems (*Supporting Information*), our experiments still provide sufficient resolution for the differences in the depth and thickness of the Pv – pPv boundaries in the studied systems.

The uncertainties in pressure scales are important to consider for comparison between different experimental results and for seismic applications. The uncertainty of the gold scale may be approximately 5 GPa (100 km) at the investigated $P-T$ range (*Supporting Information*). However, the uncertainty of the pressure difference, which is more important for the thickness and differences in transition depths between different compositions, should be less than 5 GPa.

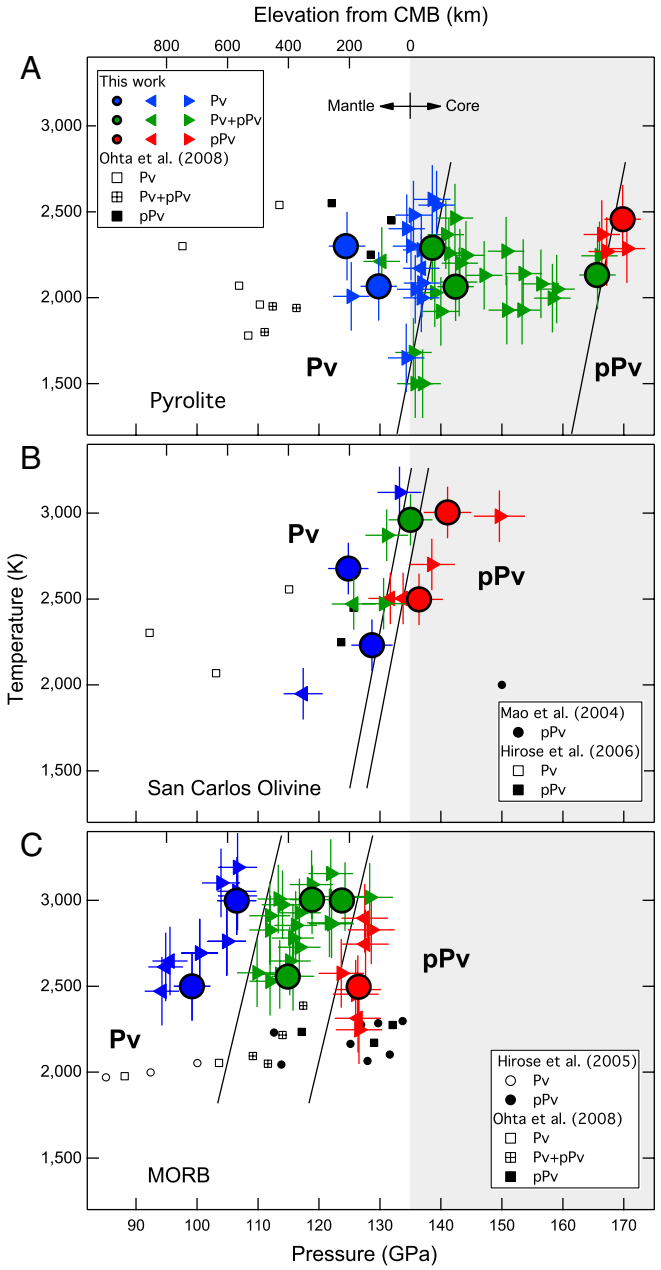

Fig. 2. The pressure-temperature conditions for the stability of Pv, Pv + pPv, and pPv in (*A*) calcium-free pyrolitic, (*B*) San Carlos olivine, and (*C*) MORB compositions. The right- and left-pointing triangles represent data points measured along the forward and reverse paths, respectively, and the large circles represent the data points obtained directly from heating of amorphous starting materials. Blue, green, and red triangles represent observations of Pv, Pv + pPv, and pPv, respectively. The solid black lines are the phase boundaries determined from our data. The Clapeyron slope of the boundary was obtained from Catalli et al. (4) (*Supporting Information*). The black symbols are the data points from previous studies in related compositions (6, 18, 23). Error bars are 1σ uncertainties.

The robust conclusions we can draw from our data considering the uncertainties are: (1) the Pv → pPv transition in a pyrolitic composition occurs deeper by 200 and 400 km than in San Carlos olivine and MORB compositions, respectively (possibly even deeper than the CMB), and (2) the Pv – pPv boundary is narrower in San Carlos olivine (<70 km) and MORB (100–300 km) compositions than pyrolite (approximately 600 km).

A calculation (4) based on an ideal solution model (19) predicted that Fe partitioning with Fp can deepen and sharpen the Pv – pPv boundary only if Fe^{2+} content follows an order of Fp > pPv > Pv (20). However, other measurements suggest Fp > Pv > pPv (17), which would sharpen the boundary as well, but push the transition to shallower depths. We found that the Pv – pPv boundary in San Carlos olivine deepens by approximately 20 GPa compared to Fp-free Fe^{2+}-bearing samples (4) and sharpens the thickness to ≤70 km, which is in excellent agreement with the calculation and supports iron preferentially partitioning into pPv over Pv (20, 21).

Whereas both our pyrolite and San Carlos olivine have similar Fe contents and mineralogy, pyrolite has a much thicker and deeper Pv – pPv boundary. In pyrolite, Fe^{2+} still partitions into the Fp, but the Pv – pPv system is rich in Al. Therefore, the difference in these two systems indicate that Al likely makes the two phase region much deeper and wider in pyrolite. This interpretation helps explain the results from recent experiments (4, 5, 7, 8) and is in excellent agreement with computations (9, 10, 12, 13) on Al effects [but not all (22)] (Fig. 3 and *Supporting Information*). Therefore, Al appears to be the key element that determines the detectability of the Pv → pPv transition in systems without a phase that participates in Al partitioning with the Mg-silicate phases.

We find that the Pv – pPv transition in MORB is shallower and narrower than in pyrolite, although MORB has more Al_2O_3 by a factor of 3–4. This seems to be in disagreement with some previous studies on Al-bearing binary or ternary systems (4, 5, 7, 8) (Fig. 3*A*), but in partial agreement with the MORB study by Ohta et al. (23). Unlike pyrolite, MORB contains separate silica phases and the CF phase that can lower the activity of Al through the partitioning into these phases. We observed that silica undergoes a gradual transition from $CaCl_2$-type to α-PbO_2-type at a pressure range similar to that of the Pv → pPv transition, consistent with a previous study on a similar composition (18). The Al_2O_3 content in silica increases by a factor of four at the $CaCl_2$-type → α-PbO_2 transition, reaching 13 wt% after the transition (18). This drastic increase in Al_2O_3 content combined with the large amount of silica in MORB would greatly affect the Pv → pPv transition. The CF phase may be a sink for both Fe and Al because it contains both FeO (10 wt%) and Al_2O_3 (37 wt%) and is a significant modal fraction (15 wt%) of MORB (18).

Previous experiments on San Carlos olivine composition (6, 24) do not constrain the thickness to a precision better than 300 km, although the data are generally in agreement with our results (Fig. 2*B*). A computational study (14) predicted a thickness of 100 km for San Carlos olivine composition, which is in good agreement with our result (Fig. 3*B*).

Two previous studies on a pyrolitic composition (17, 23) reported a much shallower and thinner Pv – pPv boundary. Although the previous studies had Ca-Pv, we did not include Ca in the system for unambiguous phase identification (*Supporting Information*). The presence of Ca-Pv in Ohta et al. (23) is unlikely the source of the discrepancy because of the low modal fraction of Ca-Pv and undetectably low amount of Al_2O_3 in Ca-Pv in their samples (17, 23). A modal calculation based on the reported composition indicates our Al_2O_3 content is slightly higher (by a factor of 1.2) in the Pv – pPv system than Ohta et al. (23). However, we do not believe this slight difference can explain the factor of five smaller thickness reported in (17, 23).

Although it is difficult to understand the source of the discrepancy, there are a few important differences to consider. We use noble gas pressure medium instead of NaCl or no pressure medium, conduct forward and reverse measurements, use anhydrous starting materials, and present results from both long and short heating durations. A small amount of sodium or water (if present) may stabilize pPv as previously suggested (9, 18) (*Supporting Information*). However, as discussed above, our results on pyrolite are much more consistent with most of the existing experi-

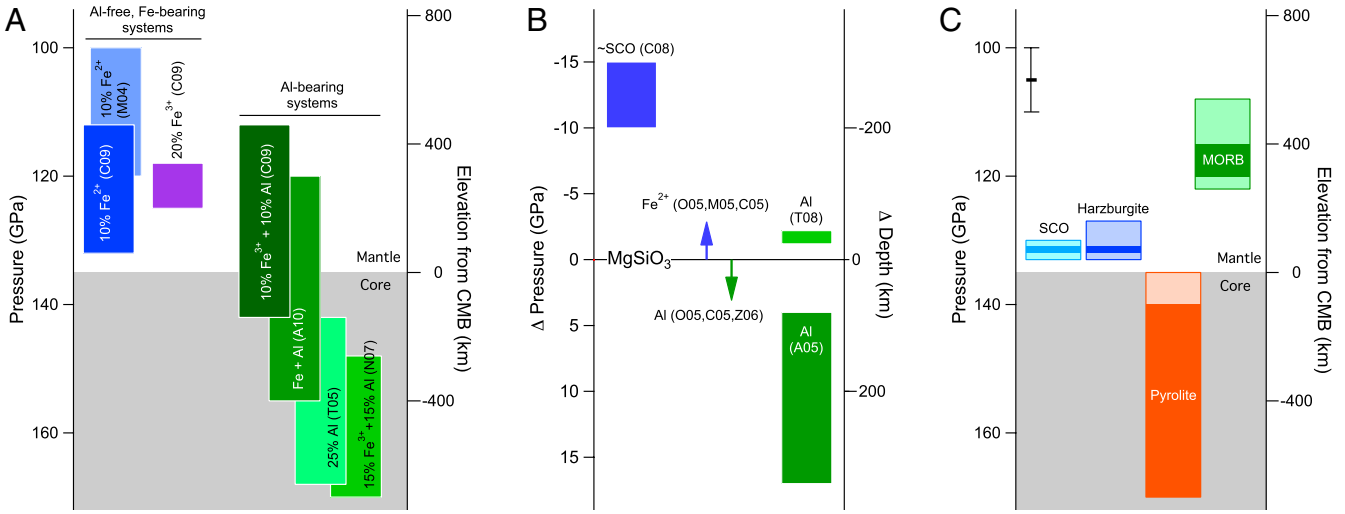

Fig. 3. Depth and thickness of the Pv – pPv boundary in binary and ternary systems reported in (*A*) experimental [C09 (4), M04 (6), A10 (5), T05 (7), N07 (8)] (*Supporting Information*) and (*B*) computational [A05 (9), O05 (10), M05 (11), C05 (12), Z06 (13), T08 (22), C08 (14)] studies, and in (*C*) multiphase, multicomponent systems reported in this study (SCO: San Carlos olivine). The locations of the bars indicate the depth range of mixed phase regions. The experimental results are plotted for a temperature of 2,500 K. The computational results are plotted with respect to their estimates on the transition pressure for $MgSiO_3$. In (*C*), the dark colored regions show the lower bound for the thickness whereas the dark and light regions together represent an upper bound obtained from Fig. 2. The error bar in (*C*) represents the uncertainty in transition depth from the pressure scale ($1\sigma = \pm 5$ GPa). The uncertainty in the thickness should be smaller, because it relies on difference in pressure within the same scale.

mental and computational results regarding the effects of Al and Fe (Fig. 3).

Our results on San Carlos olivine can be extrapolated to olivine-rich rocks such as harzburgite (4, 19). In the lower-mantle, harzburgite has slightly less Fp (40 mol%) and slightly more Al_2O_3 ($\leq$1 wt%) than San Carlos olivine. The pPv transition in harzburgite can be calculated (4) and should begin at a pressure between 125 and 130 GPa, with a thickness between 0 and 7 GPa (Fig. 3*C*). Therefore, the Pv – pPv boundary in harzburgite should be seismically detectable. The depth and thickness of the Pv – pPv boundary in harzburgite and MORB are in better agreement with the D″ discontinuity (200–400 km above the CMB) than pyrolite. In addition, given that the pressure at the CMB is 135 GPa and the gold scale we used is unlikely to overestimate pressure (*Supporting Information*), our results suggest that the Pv $\rightarrow$ pPv transition may not occur in the pyrolitic mantle (or at least will be undetectable due to the thickness), whereas it likely occurs in mantle regions rich in differentiated subducted lithosphere materials, such as MORB or harzburgite (Fig. 3*C*).

Our results show that mineralogical effects play a critical role for the detectability of the Pv – pPv boundary. In rocks with intermediate amounts of Al, where all Al exists in Pv or pPv such as pyrolite (3–5 wt% Al_2O_3), the transition may occur at higher pressures than the CMB with a mixed phase region too wide for seismic detection due to the lack of a mineral phase that can reduce the effects of Al. Aluminum-depleted and Fp-enriched rocks, such as harzburgite, will have a detectable Pv – pPv boundary. Although MORB contains much more Al, it has a narrower boundary than pyrolite due to the existence of phases that help mitigate its effects. The Pv – pPv boundary in MORB may be seismologically detectable, if lattice preferred orientation (25) and/or nonlinearity in the phase fraction (4, 19) can further decrease the seismic thickness of the boundary. Although global coverage is sparse, large regions of robust lateral extension of the D″ discontinuity have been documented in the lowermost mantle beneath the Circum-Pacific (26, 27). If subducting slabs are eventually deposited at the base of the mantle (27, 28), these areas likely have subducted materials containing harzburgite and MORB.

Geochemical studies have shown that the mantle contains significant amounts of basaltic crustal materials (29) and refractory residues of melt extraction (30). Recent petrologic evidence also suggests deep subduction of ocean crust (31). In solid mantle materials, chemical diffusion is limited to a few meters even over billion year time scales (32–34), preserving chemical heterogeneities in the deep mantle. A recent dynamic simulation (35) demonstrated that although differentiated rocks represent a small fraction of subducted material, preferential deposition can occur in the CMB region if they have sufficiently higher density than pyrolite. Over geologic time scales this could result in these rocks becoming the dominant type in the region. According to our results, the observation of the D″ discontinuity resulting from the Pv $\rightarrow$ pPv transition may indicate the presence of significant amounts of differentiated materials transported from the shallow mantle into the CMB by subducting slabs. Because the lowermost mantle is believed to be the source region of mantle plumes and the graveyard of subducting slabs, our results may have broad implications for the scale of mantle mixing, the nature of seismic heterogeneities, the source of hot spot volcanism, and the cycling of elements through the Earth's mantle.

Materials and Methods

The starting materials were a natural San Carlos olivine with a composition of $(Mg_{0.89}Fe^{2+}_{0.11})_2SiO_4$ and synthetic glasses with composition given in the *Supporting Information*. The glass starting materials were synthesized from oxide starting mixtures by the containerless method under reducing conditions to prevent iron oxidation (36). The starting materials were powdered and mixed with 10 wt% gold, used as a pressure calibrant and laser absorber. A prepressed sample + gold platelet was placed in a 35, 50, or 90 μm hole drilled into a preindented rhenium gasket using beveled diamond anvils with 75, 100, or 150 μm culets in symmetric type diamond-anvil cells, respectively. The sample platelet was separated from the diamond anvils by a few micron-sized grains of the sample material to allow the pressure medium (argon or neon) to flow around the sample and insulate it from the diamonds during laser heating (*Supporting Information*). Argon was cryogenically loaded as the pressure medium and thermal insulation, except for four MORB samples where neon was loaded using the gas-loading system at GeoSoilEnviro Center for Advanced Radiation Sources (GSECARS). The neon-loaded samples also had a approximately 5 μm ruby sphere placed at the edge of the sample chamber, well separated from the sample platelet, for pressure determination during gas loading. During X-ray diffraction measurements, pressures were determined in situ from the equation of state of gold (37). We note that the sample setup used in this study is identical to that in our previous study on mantle-related binary and ternary systems (4), facilitating an internally consistent comparison among our six different datasets on the thickness and depth of the Pv – pPv boundary.

X-ray diffraction patterns were collected at beamline 13-ID-D of the GSECARS sector of the Advanced Photon Source (APS). A total of six, four, and six different samples were prepared for pyrolitic, San Carlos olivine, and MORB starting materials, respectively. The starting materials were taken up to target pressures and then heated using the double-sided, flat-top laser heating system while simultaneously collecting diffraction patterns every 2–3 min during the heating cycle (38). Gray body radiation from both sides of the sample was collected for temperature estimation. Laser heating was performed between 1,500 K and 3,000 K in cycles of approximately 30 min to prevent overheating of the diamond-anvil cell. The sample was heated for 1–1.5 h at a given starting pressure before it was determined that the sample was well crystallized and likely in the equilibrium phase assemblage. Approximate modal abundances were determined using the starting oxide composition determined by EPMA. All diffraction patterns show clear diffraction intensities from the pressure medium, ensuring quasi-hydrostaticity and good insulation between the sample platelet and the diamond anvils (Fig. 1). Diffraction images were integrated to produce diffraction patterns using the Fit2D program (39). The diffraction patterns were used to determine the stability fields of Pv, pPv, and a mixed phase (Pv + pPv).

ACKNOWLEDGMENTS. We would like to thank R.G. Trønnes and two anonymous reviewers for helpful comments that improved this manuscript. This work is supported by a National Science Foundation (NSF) Grant (EAR0738655 and EAR1045673, S.-H.S.) and a Department of Energy (DOE) National Nuclear Security Administration Stewardship Science Graduate Fellowship (K.C.). This work was performed at the GeoSoilEnviro Center for Advanced Radiation Sources (GeoSoilEnviroCARS) sector of the Advanced Photon Source (APS), Argonne National Laboratory. GeoSoilEnviroCARS is supported by the NSF and the DOE. Use of the APS is supported by the DOE.

1. Murakami M, Hirose K, Kawamura K, Sata N, Ohishi Y (2004) Post-perovskite phase transition in $MgSiO_3$. *Science* 304:855–858.
2. Oganov AR, Ono S (2004) Theoretical and experimental evidence for a post-perovskite phase of $MgSiO_3$ in Earth's D″ layer. *Nature* 430:445–448.
3. Shim SH, Duffy TS, Jeanloz R, Shen G (2004) Stability and crystal structure of $MgSiO_3$ perovskite to the core-mantle boundary. *Geophys Res Lett* 31:L10603.
4. Catalli K, Shim SH, Prakapenka V (2009) Thickness and Clapeyron slope of the post-perovskite transition. *Nature* 462:782–785.
5. Andrault D, et al. (2010) Experimental evidence for perovskite and post-perovskite coexistence throughout the whole D″ region. *Earth Planet Sc Lett* 293:90–96.
6. Mao WL, et al. (2004) Ferromagnesian postperovskite silicates in the D″ layer of the Earth. *Proc Natl Acad Sci USA* 101:15867–15869.
7. Tateno S, Hirose K, Sata N, Ohishi Y (2005) Phase relations in $Mg_3Al_2Si_3O_{12}$ to 180 GPa: Effect of Al on post-perovskite phase transition. *Geophys Res Lett* 32:L15306.
8. Nishio-Hamane D, Fujino K, Seto Y, Nagai T (2007) Effect of the incorporation of $FeAlO_3$ into $MgSiO_3$ perovskite on the post-perovskite transition. *Geophys Res Lett* 34:L12307.
9. Akber-Knutson S, Steinle-Neumann G, Asimow PD (2005) Effect of Al on the sharpness of the $MgSiO_3$ perovskite to post-perovskite phase transition. *Geophys Res Lett* 32:L14303.
10. Ono S, Oganov AR (2005) In situ observations of phase transition between perovskite and $CaIrO_3$-type phase in $MgSiO_3$ and pyrolitic mantle composition. *Earth Planet Sc Lett* 236:914–932.
11. Mao WL, et al. (2005) Iron-rich silicates in the Earth's D″ layer. *Proc Natl Acad Sci USA* 102:9751–9753.
12. Caracas R, Cohen RE (2005) Effect of chemistry on the stability and elasticity of the perovskite and post-perovskite phases in the $MgSiO_3$-$FeSiO_3$-Al_2O_3 system and implications for the lowermost mantle. *Geophys Res Lett* 32:L16310.
13. Zhang F, Oganov AR (2006) Mechanisms of Al^{3+} incorporation in $MgSiO_3$ post-perovskite at high pressures. *Earth Planet Sc Lett* 248:54–61.
14. Caracas R, Cohen RE (2008) Ferrous iron in post-perovskite from first-principles calculations. *Phys Earth Planet Inter* 168:147–152.
15. Wysession ME, et al. (1998) *The Core-Mantle Boundary Region* (Am Geophysical Union, Washington DC), pp 273–297.
16. Lay T (2008) Sharpness of the D″ discontinuity beneath the Cocos Plate: Implications for the perovskite to post-perovskite phase transition. *Geophys Res Lett* 35:L03304.
17. Murakami M, Hirose K, Sata N, Ohishi Y (2005) Post-perovskite phase transition and mineral chemistry in the pyrolitic lowermost mantle. *Geophys Res Lett* 32:L03304.
18. Hirose K, Takafuji N, Sata N, Ohishi Y (2005) Phase transition and density of subducted MORB crust in the lower mantle. *Earth Planet Sc Lett* 237:239–251.
19. Stixrude L (1997) Structure and sharpness of phase transitions and mantle discontinuities. *J Geophys Res* 102:14835–14852.
20. Kobayashi Y, et al. (2005) Fe-Mg partitioning between $(Mg,Fe)SiO_3$ post-perovskite, perovskite, and magnesiowüstite in the Earth's lower mantle. *Geophys Res Lett* 32: L19301.
21. Auzende L, et al. (2008) Element partitioning between magnesium silicate perovskite and ferropericlase: New insights into bulk lower-mantle geochemistry. *Earth Planet Sc Lett* 269:164–174.
22. Tsuchiya J, Tsuchiya T (2008) Postperovskite phase equilibria in the $MgSiO_3$-Al_2O_3 system. *Proc Natl Acad Sci USA* 105:19160–19164.
23. Ohta K, Hirose K, Lay T, Sata N, Ohishi Y (2008) Phase transitions in pyrolite and MORB at lowermost mantle conditions: Implications for a MORB-rich pile above the core-mantle boundary. *Earth Planet Sc Lett* 267:107–117.
24. Hirose K, Sinmyo R, Sata N, Ohishi Y (2006) Determination of postperovskite phase transition boundary in $MgSiO_3$ using Au and MgO pressure standards. *Geophys Res Lett* 33:L01310, doi:10.1029/2005GL024468.
25. Ammann MW, Brodholt JP, Wookey J, Dobson DP (2010) First-principles constraints on diffusion in lower-mantle minerals and a weak D″ layer. *Nature* 465:462–465.
26. Lay T, Williams Q, Garnero EJ (1998) The core-mantle boundary layer and deep Earth dynamics. *Nature* 392:461–468.
27. van der Hilst RD, et al. (2007) Seismostratigraphy and thermal structure of Earth's core-mantle boundary region. *Science* 315:1813–1817.
28. Hutko AR, Lay T, Garnero EJ, Revenaugh J (2006) Seismic detection of folded, subducted lithosphere at the core-mantle boundary. *Nature* 441:333–336.
29. Sobolev AV, et al. (2007) The amount of recycled crust in sources of mantle-derived melts. *Science* 316:412–417.
30. Liu CZ, et al. (2008) Ancient, highly heterogeneous mantle beneath Gakkel ridge, Arctic Ocean. *Nature* 452:311–316.
31. Walter MJ, et al. (2011) Deep mantle cycling of oceanic crust: Evidence from diamonds and their mineral inclusions. *Science* 334:54–57.
32. Allègre CJ, Turcotte DL (1986) Implications of a two-component marble-cake mantle. *Nature* 323:123–127.
33. Morgan JP, Morgan WJ (1999) Two-stage melting and the geochmical evolution of the mantle: a recipe for mantle plum-pudding. *Earth Planet Sc Lett* 170:215–239.
34. Holzapfel C, Rubie DC, Frost DJ, Langenhorst F (2005) Fe-Mg interdiffution in $(Mg,Fe)SiO_3$ perovskite and lower mantle reequilibration. *Science* 309:1707–1710.
35. Nakagawa T, Tackley PJ, Deschamps F, Connolly JAD (2010) The influence of MORB and harzburgite composition on thermo-chemical mantle convection in a 3-D spherical shell with self-consistently calculated mineral physics. *Earth Planet Sc Lett* 296:403–412.
36. Tangeman JA, et al. (2001) Vitreous forsterite (Mg_2SiO_4): Synthesis, structure, and thermochemistry. *Geophys Res Lett* 28:2517–2520.
37. Tsuchiya T (2003) First-principles prediction of the $P - V - T$ equation of state of gold and the 660-km discontinuity in Earth's mantle. *J Geophys Res* 108:2462.
38. Prakapenka VB, et al. (2008) Advanced flat top laser heating system for high pressure research at GSECARS: application to the melting behavior of germanium. *High Pressure Res* 28:225–235.
39. Hammersley AP, Svensson SO, Fitch AN, Hausermann , D (1996) Two-dimensional detector software: From real detector to idealised image or two-theta scan. *High Pressure Res* 14:235–248.